Impact of future land use and land cover changes on atmospheric chemistry-climate interactions

Laurens Ganzeveld,[1,2] Lex Bouwman,[3] Elke Stehfest,[3] Detlef P. van Vuuren,[3] Bas Eickhout,[3,4] and Jos Lelieveld[2,5]

Received 11 February 2010; revised 10 August 2010; accepted 17 August 2010; published 2 December 2010.

[1] To demonstrate potential future consequences of land cover and land use changes beyond those for physical climate and the carbon cycle, we present an analysis of large-scale impacts of land cover and land use changes on atmospheric chemistry using the chemistry-climate model EMAC (ECHAM5/MESSy Atmospheric Chemistry) constrained with present-day and 2050 land cover, land use, and anthropogenic emissions scenarios. Future land use and land cover changes are expected to result in an increase in global annual soil NO emissions by ~1.2 TgN yr^{-1} (9%), whereas isoprene emissions decrease by ~50 TgC yr^{-1} (−12%). The analysis shows increases in simulated boundary layer ozone mixing ratios up to ~9 ppbv and more than a doubling in hydroxyl radical concentrations over deforested areas in Africa. Small changes in global atmosphere-biosphere fluxes of NO_x and ozone point to compensating effects. Decreases in soil NO emissions in deforested regions are counteracted by a larger canopy release of NO_x caused by reduced foliage uptake. Despite this decrease in foliage uptake, the ozone deposition flux does not decrease since surface layer mixing ratios increase because of a reduced oxidation of isoprene by ozone. Our study indicates that the simulated impact of land cover and land use changes on atmospheric chemistry depends on a consistent representation of emissions, deposition, and canopy interactions and their dependence on meteorological, hydrological, and biological drivers to account for these compensating effects. It results in negligible changes in the atmospheric oxidizing capacity and, consequently, in the lifetime of methane. Conversely, we expect a pronounced increase in oxidizing capacity as a consequence of anthropogenic emission increases.

Citation: Ganzeveld, L., L. Bouwman, E. Stehfest, D. P. van Vuuren, B. Eickhout, and J. Lelieveld (2010), Impact of future land use and land cover changes on atmospheric chemistry-climate interactions, *J. Geophys. Res.*, *115*, D23301, doi:10.1029/2010JD014041.

1. Introduction

[2] Rapid changes in ecosystems as a result of human activities, such as tropical deforestation, are of great relevance to climate and global change [*Millennium Ecosystem Assessment*, 2005]. Scenarios of future anthropogenic land cover and land use suggest continued changes as a result of the increasing demand for food and (bio)energy. Several previous studies have indicated the interactions between global land cover, the carbon cycle, and the climate system. For example, *Chase et al.* [1996] showed a significant impact on climate simulated with a general circulation model constrained by potential and present-day vegetation cover estimates. Differences in the leaf area index (LAI) induced significant changes in the boundary layer (BL) meteorology and also affected the large-scale circulation indicated by significant changes in the 200 mbar (~12 km altitude) jet stream and wave generation. These changes were caused by perturbations of tropical heating patterns associated with changes in surface latent heat fluxes (LE). An analysis by *Werth and Avissar* [2002], focusing on tropical land use and land cover changes (LUCC), indicated not only local but also significant global changes in the simulated precipitation. *Cox et al.* [2000] suggested, based on the use of a climate model coupled to an interactive vegetation and soil carbon model, that the role of the biosphere in controlling the carbon and hydrological cycles results in a climate-driven loss of tropical forest in the Amazon. The simulated increase in atmospheric CO_2 attributed to anthropogenic emissions and enhanced soil and plant respiration could result in a warming and drying and, ultimately, the loss of forest.

[3] Recent studies have additionally addressed land-cover-induced changes in energy, water and carbon exchanges, and

[1]Department of Environmental Sciences, Wageningen University and Research Centre, Wageningen, Netherlands.
[2]Max-Planck Institute for Chemistry, Mainz, Germany.
[3]National Institute for Public Health and the Environment, Netherlands Environmental Assessment Agency, Bilthoven, Netherlands.
[4]Now at European Parliament, Strasbourgh, France.
[5]The Cyprus Institute, Nicosia, Cyprus.

0148-0227/10/2010JD014041

impacts of climate and land cover changes on reactive trace gas exchanges. Several studies focused on emissions of volatile organic compounds (VOCs), notably isoprene [*Sanderson et al.*, 2003; *Lathière et al.*, 2006; *Arneth et al.*, 2007]. These analyses were motivated by potential changes in emissions of these key precursors of ozone and aerosol production and consequences on the atmospheric radiative forcing and oxidizing capacity. However, a study by *Ganzeveld and Lelieveld* [2004] indicated that understanding the impact of land cover and land use changes on atmospheric chemistry requires considering also changes in surface reactive trace gas exchanges other than precursor emissions. Simulations of tropical deforestation scenarios with a single-column chemistry-climate model showed a complex response of the system including changes in dry deposition and biogenic emissions as well as convective transport, cloud cover, and photolysis rates. The combined impact of all deforestation-induced perturbations was a relative increase in hydroxyl radical (OH) concentrations up to about 100% at 3 km altitude downwind of the deforested regions. *Ganzeveld and Lelieveld* [2004] focused their analysis on the short-term and local-scale process interactions. Here, we discuss the results of a global-scale analysis of the long-term impact of land cover and land use changes on atmospheric chemistry-climate interactions.

[4] Our goal is to identify the relevant interactions between atmospheric chemistry processes and climate resulting from global land cover and land use changes. We do not particularly aim to arrive at a quantitative assessment of the impact of land cover and land use changes on atmospheric chemistry and climate. A recent study by *Pitman et al.* [2009] demonstrated that still large uncertainties exist with respect to quantitative analysis of the impact of land cover and land use changes on physical climate, partly resulting from different methodologies to implement land cover and land use changes in climate models. Analysis of simulated changes in climate in response to land cover and land use changes by seven climate models showed results that were statistically significant in particular regions, but with different signs among the models.

[5] For our study, we applied a coupled chemistry-climate model forced by land cover and land use projections and emission scenarios for the energy/industry sectors that have been compiled with an integrated assessment model. We performed three time slice experiments with the chemistry-climate model: one experiment reflecting present-day conditions, one experiment that used only the 2050 land use and land cover, and one experiment that used land cover and land use and anthropogenic emissions for 2050.

[6] More details on the setup of the simulations, including the applied chemistry-climate model and the land cover, land use, and anthropogenic emission scenarios, are presented in section 2, followed by an analysis of the global and regional changes in surface exchanges and atmospheric chemistry in section 3.

2. Simulation Setup

2.1. Chemistry-Climate Model

[7] The analysis is based on simulations with the Modular Earth Submodel System [*Jöckel et al.*, 2005, 2006] coupled to the General Circulation Model ECHAM5 [*Roeckner et al.*, 2003], referred to as EMAC (ECHAM5/Modular Earth Submodel System Atmospheric Chemistry model). We applied EMAC version 1.6 to conduct simulations at a T42 spectral resolution (~2.8°) with 31 vertical levels. EMAC contains a detailed representation of surface reactive trace gas and aerosol exchanges, a state-of-the-art representation of tropospheric and stratospheric gas-phase chemistry [*Sander et al.*, 2005], and scavenging [*Tost et al.*, 2006]. Prescribed emissions in the default setup of EMAC for present-day simulations are based on the Emission Database for Global Atmospheric Research (EDGAR; http://www.mnp.nl/edgar/) version 3.2 fast-track update of the emission inventory for the year 2000 [*Olivier et al.*, 2005; *van Aardenne et al.*, 2005]. In our analysis, the contribution by anthropogenic emissions in total emissions for present day and the future is based on the emissions compiled with the Integrated Model to Assess the Global Environment (IMAGE) [*Alcamo et al.*, 1998; *Bouwman et al.*, 2006].

[8] The interactively simulated source, sink, and tracer transport processes are driven by the meteorological and hydrological parameters from ECHAM5. The parameters most relevant for our analysis are turbulence; radiation; air, surface, and soil temperatures; soil moisture; precipitation; and the surface cover fractions of water, bare soil, snow ice, and wet and dry vegetation.

[9] The setup of simulations has been determined mainly by the aim to assess process interactions induced by land use and land cover changes on atmosphere-biosphere exchanges, but we have ignored at this stage long-term changes in the climate attributed to increases in greenhouse gases, aerosols, and changes in sea surface temperature and sea-ice cover. The latter would require an ensemble of transient simulations that is not yet feasible because of limitations in terms of the number and duration of the CPU-intensive integrations. Actually, we limit the analysis presented here to the last 4 years of the simulations, which covered 5.5 years in total. Simulations for the first 1.5 years used an implementation of soil-biogenic NO emissions, which resulted in a too large global annual soil NO emission flux >25 Tg NO-N (see also section 3.2.1).

[10] In our simulations, we use land cover, land use, and anthropogenic emission data for the years 2000 and 2050 from the IMAGE model implementation of the International Panel on Climate Change Special Report on Emission Scenarios (SRES) A2 scenarios [*IMAGE team*, 2001; *Strengers et al.*, 2004]. The first simulation, hereafter referred to as IMG-2000, reflects present-day conditions and uses land cover, land use, and anthropogenic emissions for the year 2000. The second simulation, referred to as IMG-2050-lucc, is based on land use and land cover data for 2050 but uses the present-day anthropogenic emissions. The third simulation, referred to as IMG-2050-lucc&emis, is based not only on the 2050 land use and land cover but also uses the 2050 anthropogenic emissions scenario.

[11] In our analysis, we address the impact of land cover and land use changes on gas-phase exchange and chemical processes, concentrating on the role of changes in the atmospheric oxidation capacity and its consequences for the lifetime of methane. The selected chemistry scheme of the gas-phase submodule Module Efficiently Calculating the Chemistry of the Atmosphere [*Sander et al.*, 2005] includes the background methane (CH_4), carbon monoxide

(CO), nitrogen oxides (NO_x, NO + NO_2), and ozone (O_3) chemistry, and that of nonmethane hydrocarbons including the role of isoprene (C_5H_8) and oxidation products such as methyl vinyl ketone, methacroleine, formic and acetic acid, and acetone. One particular modification of the gas-phase chemistry relevant to the present analysis is the introduction of an extra source of OH to simulate OH concentrations in the tropical boundary layer comparable to observed concentrations [*Lelieveld et al.*, 2008]. This assumes the production of two OH molecules in the reaction between the isoprene peroxy radical (ISO2) with the peroxy radical (HO_2) forming ISOOH (T. Butler, personal communication, 2008).

[12] The impacts of changes in ozone on radiative forcing are not considered in these simulations, which means that the IMG-2050-lucc&emis and IMG-2050-lucc simulations are based on the same meteorological and hydrological drivers for surface exchanges for 2050 land cover and land use.

[13] The simulations of surface reactive trace gas exchange include natural emissions, dry deposition, and canopy interactions involving in-canopy chemistry and turbulent exchange. Further details of the modeling of these processes with a multilayer canopy exchange model are given by *Ganzeveld et al.* [2002, 2006]; here we discuss only some particular features relevant to the present study. Soil-biogenic NO_x and biogenic VOC emissions are calculated interactively in the EMAC submodel EMDEP (Emissions and Deposition). Soil-biogenic NO_x emissions are calculated using a modified version of the algorithm by *Yienger and Levy* [1995]. This has previously been implemented and applied, in combination with the multilayer canopy exchanges model, in the chemistry-climate model ECHAM4 to study the role of canopy processes for global soil-biogenic NO_x emissions [*Ganzeveld et al.*, 2002]. The multilayer canopy exchanges model, which considers dry deposition, biogenic emissions, and the extinction of radiation and turbulence distinguishing a crown and understory layer, has been applied in this study to consider NO_x as well as VOC canopy interactions. *Ganzeveld et al.* [2002] considered NO emissions from artificial nitrogen (N) fertilizer application. Since N fertilizer application is not the only source of enhanced NO emissions from land use systems, we also include animal manure application. The approach for distributing N fertilizer use and animal manure inputs is described in detail by *Bouwman et al.* [2006]. An additional difference with the study by *Ganzeveld et al.* [2002] is that the emission factor for NO emissions associated with fertilizer and animal manure application is reduced from 2.5% [*Yienger and Levy*, 1995] to 0.7%. This lower emission factor has been derived from a more recent analysis of a large measurement data set [*Bouwman et al.*, 2002].

[14] Isoprene emissions are calculated according to the algorithm by *Guenther et al.* [1995], hereafter referred to as G95. We are aware of the more recent Model of Emissions of Gases and Aerosols from Nature [*Guenther et al.*, 2006] algorithm, which has already been implemented and evaluated in a single-column chemistry-climate model [*Ganzeveld et al.*, 2008] and will be implemented in EMDEP. However, in this analysis we apply the G95 algorithm, as the global isoprene source strengths of G95 and Model of Emissions of Gases and Aerosols from Nature are comparable (~500–600 TgC yr^{-1}). Another important motivation to apply the G95 implementation in EMAC is that it has been extensively evaluated [*Pozzer et al.*, 2007].

2.2. Land Cover, Land Use, and Anthropogenic Emission Scenarios

[15] Within the set of SRES scenarios, the A2 scenario represents a high emission scenario with a large expansion of agricultural area in contrast to other SRES scenarios that show a smaller expansion or even a decrease [*Nakicenovic et al.*, 2000; *IMAGE team*, 2001; *Strengers et al.*, 2004]. This increase in agricultural area mainly is due to a large increase in global population, reaching 11 billion in 2050, and a low level of globalization, which is assumed to lead to low exchange of technology between high- and low-income countries. The large global population combined with a slow increase in crop yields in developing countries lead to further increases in agricultural areas during the 2000–2050 period. The changes in emissions and land use are, however, within the ranges in literature [e.g., *van Vuuren and O'Neill*, 2006]. As such, this scenario is very suitable for the analysis within this study. It should be noted that a new set of scenarios proposed for climate analysis [*Moss et al.*, 2010] shows a comparable trend in one of the scenarios called RCP-8.5. For relevant parameters, such as population and income levels, the IMAGE SRES scenarios comply with the harmonization criteria described in the SRES report.

2.2.1. Land Cover and Land Use

[16] Assessment of the impact of land cover and land use changes on climate through changes in micrometeorology has generally been limited to the impact associated with albedo changes. In our analysis, we assess the impact of land use and land cover changes on atmospheric chemistry and climate considering the changes in a large number of biogeophysical and biochemical properties inferred from the IMAGE land cover and land use change scenarios. To date, IMAGE is the only model that has been used to compile spatially explicit emission and land use and land cover scenarios for all SRES scenarios. The IMAGE land cover and land use scenarios are consistent with the EDGAR emission inventory, which is commonly used to prescribe present-day emissions in EMAC and many global atmospheric chemistry and climate models. This consistency allows an optimal comparison of the impact of present-day and future projections of land use and land cover changes relative to changes in anthropogenic emissions.

[17] Not all biogeophysical and biochemical parameters relevant to the simulation of surface exchange processes in EMAC are provided by IMAGE. These parameters have been inferred by assigning ecosystem-specific parameters to the 20 ecosystem and land cover types distinguished by the IMAGE model. The parameters needed to constrain the biogenic emissions, dry deposition, canopy exchanges, and micrometeorology simulations are the amount of biomass, expressed by foliar density (g m^{-2}) and LAI, the vertical distribution of LAI (leaf area density profiles), canopy height, surface roughness, and ecosystem-specific emission factors for the calculation of biogenic VOC and NO emissions. In addition, simulation of soil-biogenic NO_x emissions uses the global distribution of agricultural land use and N inputs from fertilizers and animal manure. The N inputs simulated by the IMAGE model have a 0.5° × 0.5° resolution. In this study, we use N inputs for arable land and grassland

Table 1. Global Annual Prescribed Emissions (Total Technological and Biomass Burning, Excluding the Soil-Biogenic, Aircraft and Lightning Contribution) Per Chemical Compound Applied in the IMG-2000 and IMG-2050-lucc&emis Simulations[a]

Compound	IMG-2000	IMG-2050-lucc&emis	Biogenic
NO_x	38.5	61.2	-[b]
CO	460.7	592.8	48.2
SO_2	79	121.4	-
C_2H_4	8.7	14.1	10.7
C_2H_6	6.7	10.8	0.4
C_3H_6	3.8	6.1	3.0
C_3H_8	8.7	14	0.3
C_4H_{10}	67.8	110	0.3
CH_3CHO	2.3	3.8	0.0
CH_3COCH_3	3.0	4.9	25.6
CH_3COOH	5.4	8.7	1.4
CH_3OH	4.8	7.8	23.2
HCHO	2.7	4.4	0.0
HCOOH	1.9	3.2	1.5
MEK	6.3	10.2	0.0

[a]Units are in Tg C, N, or S. These anthropogenic emissions are complemented with a data set of global biogenic emissions for a selection of compounds.
[b]Calculated interactively.

separately because of large differences in the intensity of land use between these crop and livestock production systems [*Bouwman et al.*, 2005]. We aggregated the IMAGE fields to the EMAC grid, though maintaining the crop-grass distribution. Specific information on changes in forest, grass, and crop land cover between 2050 and the present day that was applied in the present study is provided in section 3.1.

[18] The foliar density is inferred from IMAGE's leaf biomass pool, defined in mg C km^{-2} and recalculated to g biomass m^{-2} using a typical ratio of g C (g biomass)$^{-1}$ of 0.44, according to *Lieth* [1975]. A main limitation of the biomass simulations by IMAGE is the lack of a seasonal cycle. For calculating surface reactive trace gas exchange, we need monthly mean leaf/needle biomass estimates [*Ganzeveld et al.*, 1998, 2002]. To obtain these monthly biomass estimates, we have imposed the seasonal cycle in biomass inferred from a normalized differential vegetation index climatology combined with the Olson ecosystem database (1992) [*Ganzeveld et al.*, 2002, 2006]. The relative difference between the monthly mean and the annual mean biomass estimates inferred from the normalized differential vegetation index and the Olson ecosystem distribution has been used to scale the global distribution of biomass according to the present day and 2050 IMAGE land cover distribution. This approach includes the use of ecosystem- and location-specific seasonal cycles to secure appropriate consideration of growing season characteristics.

[19] Other canopy structure properties relevant to surface trace gas exchange processes such as the vertical distribution of biomass, canopy height, and vegetation roughness have been defined based on the year 2000 and 2050 global distribution of IMAGE ecosystems and their canopy structure properties. Definition of these specific canopy structure properties (e.g., canopy height, roughness) to the IMAGE ecosystem classes has been done reducing the 72 classes of the Olson 1992 ecosystem database to the 20 IMAGE ecosystem classes. The specific land cover properties that have been modified for this analysis by replacing EMAC's vegetation properties with those based on IMAGE are forest fraction, LAI, local vegetation roughness, and albedo. The latter is modified based on the difference between the EMAC forest fraction and that of IMAGE.

2.2.2. Anthropogenic Emissions

[20] Anthropogenic emissions of greenhouse gases and air pollutants are calculated in IMAGE by multiplying activity data with emission factors. Note that hereafter the term "anthropogenic emissions" refers to industrial, technological, and biomass burning emissions. The emission factors are based on the EDGAR database for the historical period, and future emission factors evolve on the basis of the scenario assumptions. In general, emission factors decline over time, reflecting technological developments and efforts to prevent emissions with rising income levels. The activity levels in IMAGE, reflected by energy consumption and production and agricultural activities, are based on implementation of the SRES scenarios. As stated previously, the A2 scenario applied in our analysis is characterized by a low level of globalization that is assumed to lead to a low technology change with low-income countries. Moreover, the focus on the use of domestic energy resources implies relatively high shares of coal in the energy mix of India and China. This all results in relatively high levels of greenhouse and air pollutant emissions.

[21] Emissions are calculated in IMAGE at the level of 17 global regions. For the present purpose, total emissions from these regions have been downscaled to a 0.5 × 0.5 grid. The downscaling method has been described by *van Vuuren et al.* [2007]. For 2000, the geographically explicit data of the EDGAR data set were used. The 2050 emissions have been derived by downscaling the IMAGE data first to the country level, based on trends in population and income, and next to the grid harmonizing the original IMAGE output to the EDGAR data. This has been done separately for energy and industry emissions and for agricultural and biomass burning emissions. To indicate increases in the A2 scenario anthropogenic emissions, the prescribed present-day and 2050 global annual anthropogenic emissions of reactive trace gases considered in our study are listed in Table 1. Also shown are the prescribed biogenic VOC emissions from EMAC that complement the interactively simulated emissions of isoprene. Differences between the present-day EDGAR and IMAGE anthropogenic emissions are relatively small, providing confidence in the applied methodology to produce the spatially explicit anthropogenic emission inventory with IMAGE. The IMAGE SRES A2 anthropogenic emissions of NO_x, CO, SO_2, and VOC are expected to increase by 60%, 29%, 54%, and 62%, respectively, between the present day and 2050. Of the total present-day NO_x, CO, SO_2, and VOC anthropogenic emissions, respectively, 80%, 35%, 97%, and 69% originate from energy-related and industrial processes, whereas the remaining emissions are associated with biomass burning. In 2050, these numbers are expected to have changed to 88%, 47%, 99%, and 81%, indicating that most of the increase in emissions comes from changes in the energy and industrial sector.

3. Results

[22] In the following analysis of the impact of land cover and land use changes on surface exchange, atmospheric

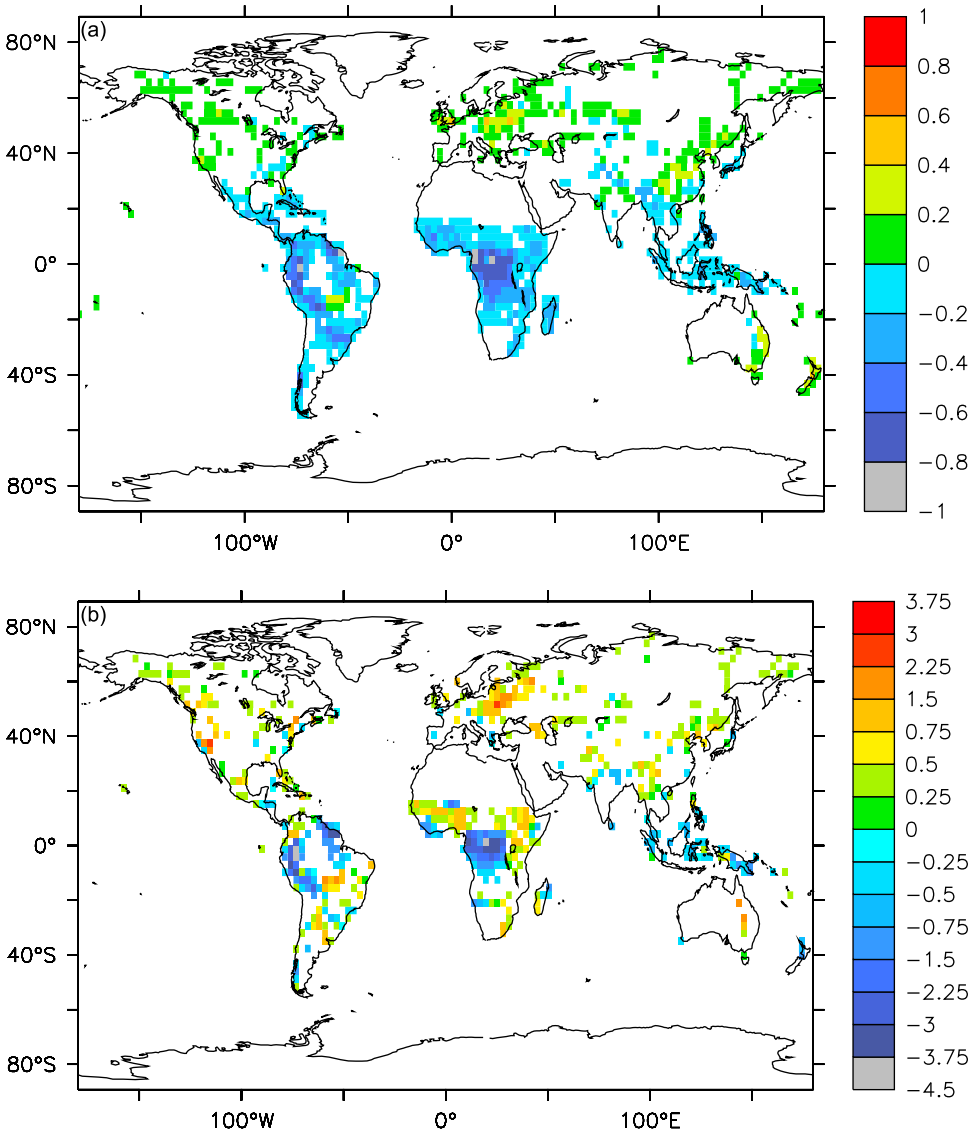

Figure 1. Absolute difference between the future and present-day 4 year mean (a) forest fraction (0–1) and (b) LAI (m^2 m^{-2}) (calculated as IMG-2050-lucc – IMG-2000). Note the nonlinear scale in LAI changes.

chemistry, and climate, we focus on regions with changes in selected parameters larger than 5% of the maximum (or minimum) of the selected range, unless stated differently. In addition, the graphical output generally reflects the 4 year mean of the parameter values sampled output at a 25 h frequency. This output frequency has been selected to reduce the large amount of model diagnostics but still allows the analysis of month-specific diurnal cycles in surface and boundary layer exchanges.

3.1. Land Cover and Land Use Changes

[23] Changes in forest, managed grassland, and cropland between the present day and 2050, according to the SRES A2 scenario, are about −21%, +23%, and +11%, respectively. Global forest cover, including temperate forest, tropical forest, and woodland and savannah, decreases from its present-day value of ~36% of the global land area (47×10^6 km^2) to ~28% (38×10^6 km^2) in 2050. These results actually reflect the net effect of deforestation and afforestation; the area of forest loss between the present day and 2050 adds up to ~10×10^6 km^2. The total change in grassland and cropland cover between the present day and 2050 is actually slightly larger than the deforested area, ~11×10^6 km^2, because agricultural land also expands in other natural ecosystems such as areas of natural grassland and savannah.

[24] Figures 1a and 1b show the changes in the global distribution of the forest fraction (0–1) and LAI, respectively, between the 2050 and 2000 SRES A2 land cover and land use scenarios. Over most of the Northern Hemisphere (NH), the forest fraction increases only moderately with some more locally significant increases >0.2 (e.g., along the West Coast of the United States and Canada and in eastern Europe). More significant decreases less than −0.2, indicating substantial deforestation, are found in the tropics and subtropics in South America and Africa. According to the IMG-2050-lucc scenario, all forest in central Africa, indi-

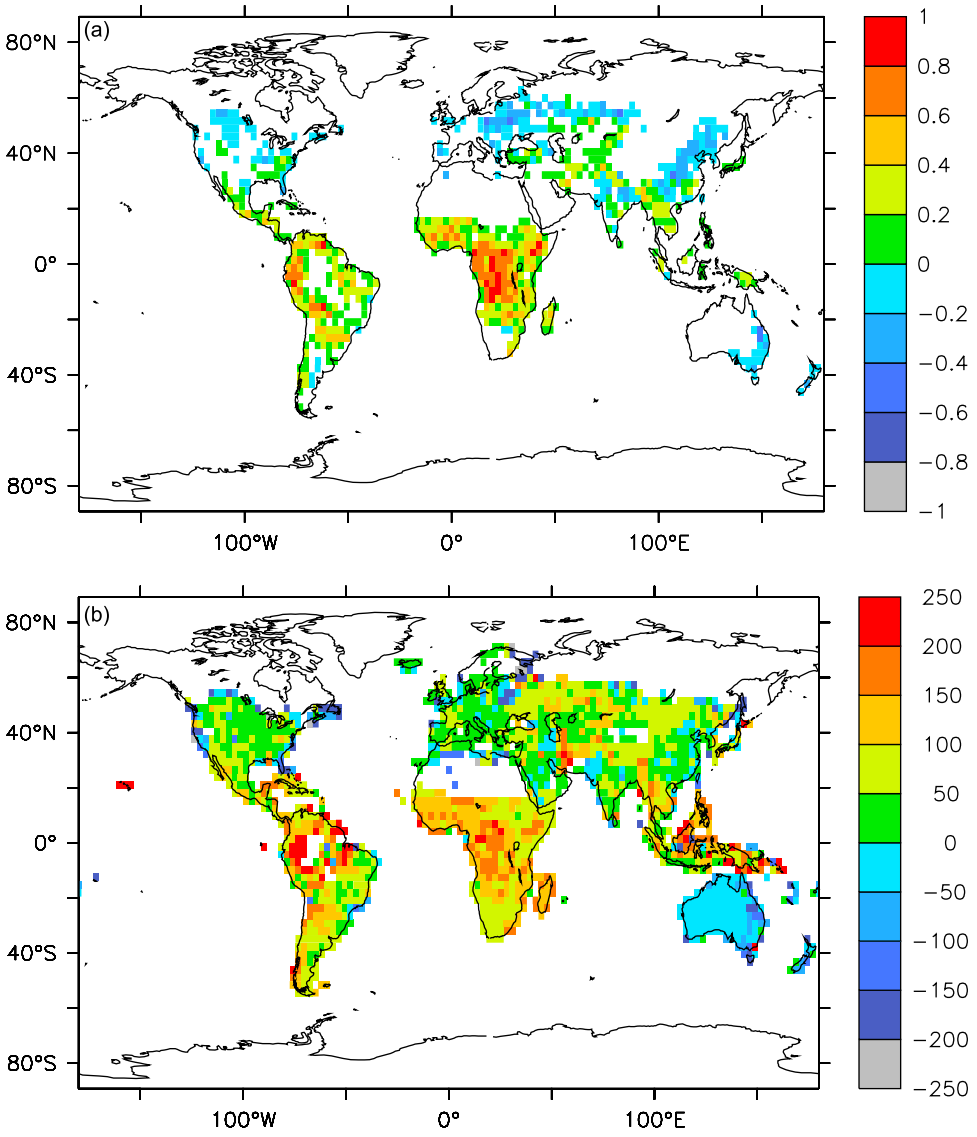

Figure 2. Absolute difference between the future and present-day 4 year mean (a) cultivation intensity (0–1) and relative difference (%) between future and present-day 4 year mean (b) application of fertilizers and animal manure on cropland and grassland (calculated as IMG-2050-lucc – IMG-2000).

cated by a change in forest fraction of about −1, will be cleared between 2000 and 2050. These changes in forest fraction are also partly reflected by a decrease in annual mean LAI of deforested areas in South America and Africa between 1 and 4 m^2 m^{-2}. These absolute decreases resemble relative decreases larger than 50% with a maximum tropical rain forest LAI of ~7 m^2 m^{-2}. The increase in LAI in the central Amazon basin in the IMG-2050-lucc scenario reflects the combined result of the absence of deforestation and an IMAGE-simulated increase in biomass associated with the CO_2 fertilization effect for an increase in CO_2 from 373 ppmv in 2000 to 537 ppmv in 2050 according to the SRES A2 scenario. Note that, compared to the studies by the *IMAGE team* [2001] and *Strengers et al.* [2004], the CO_2 fertilization effect in IMAGE has been revised downward to consider more recent insights in this process. In addition, the CO_2 fertilization effect has only been explicitly considered in the IMAGE model simulations and not in the EMAC climate simulations where the concentrations of CO_2 and that of other greenhouse gases have been prescribed at the present-day level. The deforestation in tropical and subtropical South America outside the central Amazon basin results in predicted substantial decreases in LAI for a large part of South America. In the NH, there are vast areas (e.g., along the west coast of North America) where the IMG-2050-lucc scenarios show a significant increase in LAI compared to present-day conditions. These increases reflect the simulated increase in biomass caused by climate change for the predicted relatively small increases in forest cover. In particular, high-latitude ecosystems (60–90°N) show a substantial increase in LAI, with the maximum mean summer LAI increasing from ~1.5 to ~3.5 m^2 m^{-2}. This increase largely "compensates" for the decrease in the mean tropical and subtropical (30°S–30°N) LAI from ~3.5 m^2 m^{-2} for the present day to ~2.6 m^2 m^{-2} in 2050, whereas the mean LAI in temperate regions (30–60°N and 30–60°S) does not change

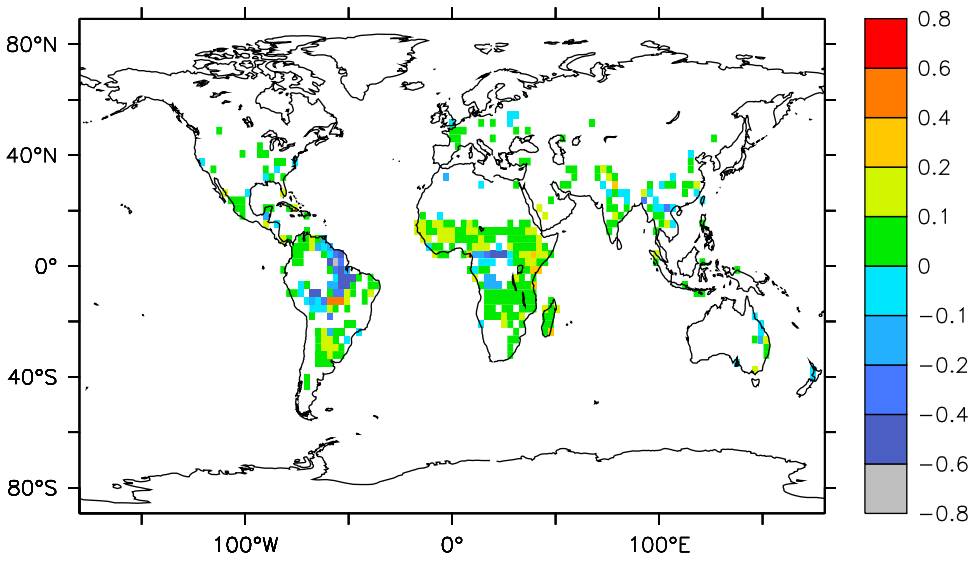

Figure 3. Absolute difference between the future and present-day 4 year mean soil NO emission flux (10^{15} molecules m^{-2} s^{-1}) (calculated as IMG-2050-lucc – IMG-2000).

significantly. As a result, the global annual mean LAI decreases from its present-day value of ~2.7 m^2 m^{-2} to ~2.2 m^2 m^{-2} in 2050.

[25] The key land use properties relevant to reactive trace gas exchanges in this study are the distribution of agricultural fields, the cultivation intensity (ranging between 0 and 1 indicating the fraction of land being used for agriculture), and the application of fertilizers and animal manure. These latter two parameters are considered in the simulations of soil NO emissions, whereas the distribution of agricultural fields, inferred from the IMAGE land cover scenarios, determines the distribution of soil NO and VOC emission factors. Figure 2a shows changes in the IMG-2050-lucc cultivation intensity scenario compared to the IMG-2000 scenario and indicates large anticipated increases in agricultural activity in the SRES A2 scenario, in particular in the tropics and subtropics in South America, Africa, western Australia, and central Asia. There are only a few locations (e.g., northeastern Europe and India) where a decrease in agricultural activity is expected in 2050 compared to the present. Relative changes in fertilizer and manure application between the IMG-2000 and IMG-2050-lucc scenarios (Figure 2b) indicate that there are large increases in the application of fertilizers and animal manure in regions with a large increase in agricultural activity. Despite rapid activity increases in, for instance, central Africa, application rates remain substantially smaller than in developed countries. The large relative increases in fertilizer and animal manure application are also reflected by an increase in the global N application in the form of fertilizers and animal manure from ~170 TgN yr^{-1} in 2000 to ~300 TgN yr^{-1} in 2050. With an assumed fractional NO loss rate of 0.7%, it indicates an increase in global soil NO emissions associated with an increase in fertilizer and animal manure application of ~0.9 TgN yr^{-1}.

3.2. Surface and Boundary Layer Exchange

[26] The above land cover and land use changes according to the SRES A2 scenario affect the micro and boundary layer meteorology (e.g., surface radiation, wind speed, and temperature), which in turn affect the biogenic emissions and dry deposition and in-canopy interactions between these emissions, deposition, and chemistry and the resulting effective atmosphere-biosphere exchange of NO_x and VOCs. Consequently, to assess LUCC-induced changes in NO_x and VOC canopy-top fluxes requires us to also evaluate, besides changes in biogenic emissions, changes in dry deposition, in-canopy chemistry, and meteorological drivers of atmosphere-biosphere exchange. Note that there will also be changes in the interactively simulated lightning NO_x emissions. However, in this analysis we focus on changes in atmosphere-biosphere exchange processes.

3.2.1. Biogenic Emissions

[27] The simulated present-day global annual soil NO-N emission flux of 13.2 Tg NO-N yr^{-1} includes the enhancement of the soil NO emissions by fertilizer and animal manure application and the so-called "pulsing," which is the enhancement in emissions attributed to precipitation after a dry period [*Yienger and Levy*, 1995]. Fertilizer and animal manure application and pulsing contribute, respectively, ~1.3 and ~2 Tg NO-N yr^{-1} to the present-day global annual soil NO emission flux. Figure 3 shows the simulated changes between the 2050 and the present-day soil NO emission flux associated with changes in NO emission potential, cultivation intensity, application of fertilizers and animal manure, and soil temperature, moisture, and precipitation. Over large regions (e.g., in central Africa and along the southeastern periphery of the Amazon rain forest), the model simulates a substantial decrease in soil NO fluxes. This decrease occurs despite the substantial increase in cultivation intensity and relatively large increases in fertilizer and animal manure application. Higher fertilizer and manure application rates appear to compensate only partly for the decrease in emission potential because of the conversion of present-day rain forest to cropland and grassland in 2050. In the model by *Yienger and Levy* [1995], tropical rain forest has an emission potential of 2.6 and 8.6 ng NO-N m^{-2} s^{-1} for wet and dry

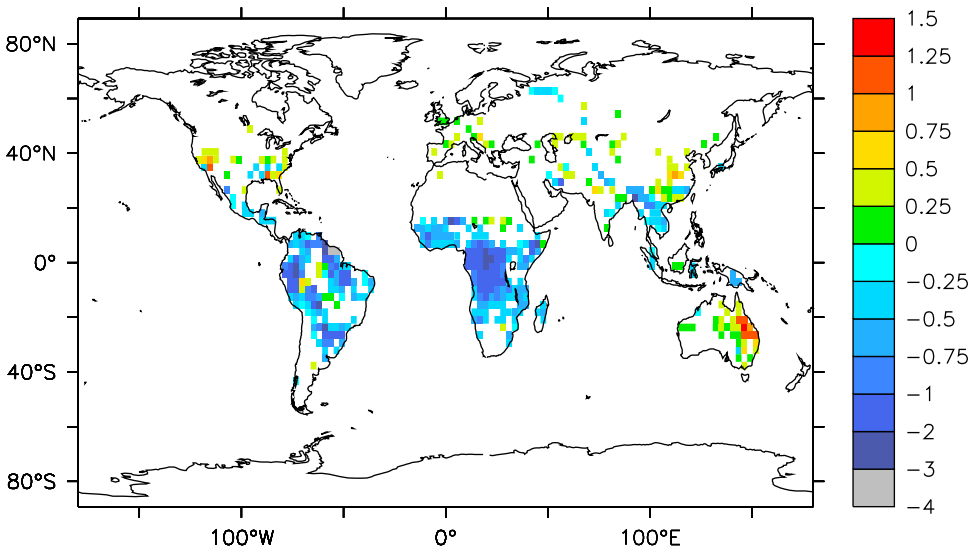

Figure 4. Absolute difference between the future and present-day 4 year mean isoprene emission flux (10^{15} molecules m^{-2} s^{-1}) (calculated as IMG-2050-lucc – IMG-2000). Note that the scale is not linear.

soils, respectively, while cropland and grassland have a basal emission potential of 0.36 ng NO-N m^{-2} s^{-1}. For the tropical and subtropical grassland regions with an anticipated increase in the application of fertilizers and animal manure (e.g., eastern South America, eastern Africa, and the western Sahel), the model simulates an increase in soil NO emissions for the year 2050 compared to present-day conditions. The overall increase of ~9% in the global annual soil NO source for 2050 (14.4 Tg NO-N yr^{-1}) compared to the present day reflects a decrease in the global emission potential caused by tropical deforestation being compensated by an increase in soil NO emissions from 1.2 to ~2.2 Tg of NO-N yr^{-1} in 2050 associated with fertilizer and animal manure application. Simulated changes in global precipitation between the present day and 2050 as a result of land cover and land use changes are negligible. However, because of simulated changes in the distribution and intensity of precipitation, there is a small simulated increase in the contribution by pulsing to NO emission fluxes from ~2 Tg of NO-N yr^{-1} for the present day to ~2.2 Tg of NO-N yr^{-1} in 2050.

[28] The land use and land cover changes result in changes between the simulated present-day and 2050 isoprene emissions (Figure 4), with a quite different spatial distribution compared to the soil NO emission changes. This also points to a different role of biogeophysical and biochemical drivers in controlling biogenic NO and VOC emissions. In central Amazonia, an increase in biomass according to the IMG-2050-lucc scenario partly explains a simulated increase in isoprene emissions for the year 2050 compared to the present day. On the other hand, the extensive deforestation in central Africa results in a strong future decrease in isoprene emissions. The substantial increases in isoprene emissions in other regions (e.g., eastern Brazil, Australia, and the United States) require a more detailed analysis of the other drivers besides biomass (e.g., net radiation) that controls isoprene emission as simulated by the G95 algorithm (see below). The overall impact of the land cover and land use changes on the global annual isoprene budget is a decrease in the simulated source strength of ~395 to 346 TgC yr^{-1} (−12%) between 2000 and 2050. Note that this difference is smaller than the difference in the global annual isoprene emission flux simulated using the default Olson 1992 ecosystem distribution (~500 TgC yr^{-1}) compared to the IMG-2000 land cover distribution. This is consistent with a study by *Guenther et al.* [2006] that also indicated that the uncertainty in global isoprene emissions associated with the applied land cover map is larger than the projected future changes in isoprene because of climate change.

3.2.2. Dry Deposition

[29] Figure 5 shows the simulated changes between the IMG-2050-lucc and IMG-2000 O_3 deposition velocity (V_{dO3}, cm s^{-1}). The dry deposition velocity of each compound (V_{dX}) is calculated diagnostically from the surface flux and surface layer concentration (molecules cm^{-3}; reference height of ~34 m) ($V_{dX} = F_X/C_X$). The surface flux over vegetation with a canopy height >1 m reflects the canopy-top flux (F_X, molecules cm^{-2} s^{-1}), explicitly simulated with the multilayer canopy exchanges model, whereas over low vegetation and nonvegetated surfaces the surface flux is calculated according to the "big-leaf" approach ($F_X = V_{dX} \times C_X$, with V_{dX} being calculated from the aerodynamic, quasi-laminar boundary layer and surface resistances [*Ganzeveld et al.*, 1998]). Future deforestation in South America, Africa, and Asia induces a decrease in V_{dO3} with maximum reductions of ~0.3 cm s^{-1} over central south Africa (Figure 5a). These changes in V_{dO3} partly reflect decreases in turbulent transport associated with a smaller roughness for agricultural fields compared to forests. The significance of a decrease in turbulent transport in explaining the decrease in V_{dO3} can be inferred from the simulated changes in the nitric acid deposition velocity (V_{dHNO3}). It is mainly controlled by turbulent transport because of an assumed negligible vegetation uptake resistance [e.g., *Wesely and Hicks*, 2000]. In contrast to the differences between the 2050 and present-day V_{dO3}, which are mostly confined to the continents, Figure 5b shows that

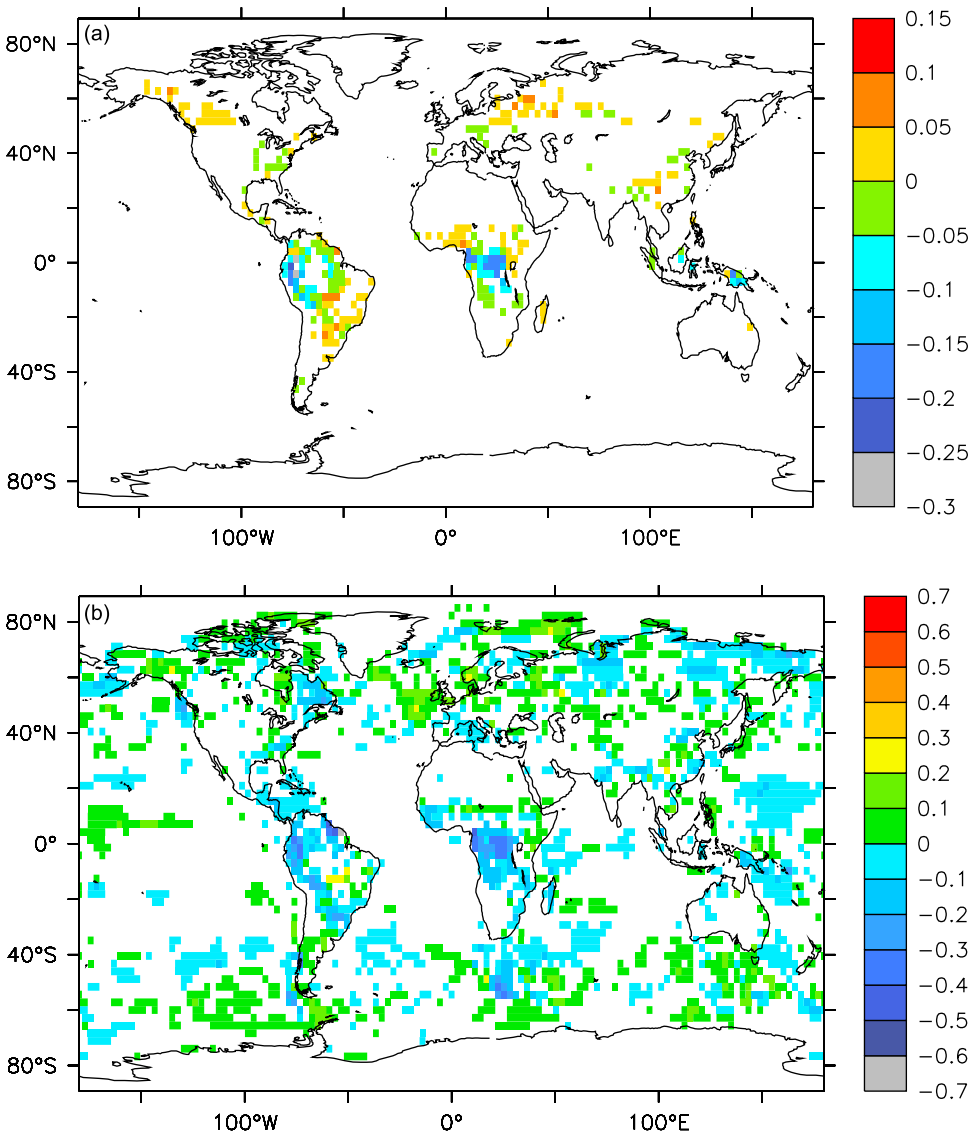

Figure 5. Absolute difference between the future and present-day 4 year mean (a) O_3 and (b) HNO_3 dry deposition velocity (V_d, cm s^{-1}) (calculated as IMG-2050-lucc – IMG-2000).

simulated changes in turbulent exchange associated with changes in atmospheric circulation result in changes in the removal of HNO_3 over the oceans remote from the regions where land cover and land use changes occur. In regions where major land cover and land use changes occur (e.g., South America and Africa), there are significant decreases in the 4 year mean V_{dHNO3} up to about 0.7 cm s^{-1} (>50% decrease). The decrease in turbulent transport only partly explains the simulated decreases in O_3 dry deposition velocity, which is mainly controlled by the stomatal uptake. This uptake depends on other surface and micrometeorological factors such as biomass, net radiation, and soil moisture. Analyzing the correlation between the changes in these drivers of stomatal uptake and changes in simulated V_{dO3} between 2000 and 2050 land cover and land use shows the highest correlation (r^2 = 0.53) between changes in LAI and V_{dO3}. However, the overall small correlation indicates a rather complicated response of dry deposition of O_3 and that of other gases for which dry deposition is also controlled by surface uptake processes, to changes in land cover and land use.

3.2.3. Meteorology

[30] To facilitate the interpretation of the mechanisms responsible for local and distant changes in surface exchanges associated with land cover and land use change, we focus, unless stated differently, our additional analysis on the regions with an absolute change in forest fraction larger than 0.05. Figure 6 shows simulated changes in surface net radiation, being an important driver of biogenic VOC emissions and stomatal exchange and, consequently, of dry deposition. Substantial increases in net radiation occur in South America and Africa between 2000 and 2050. The conversion of tropical forest to agricultural areas results in a large increase in albedo, whereas reforestation in midlatitude to high-latitude regions in the NH generally results in a decrease of the albedo between 2000 and 2050. However, there is no significant correlation between 4 year mean changes in albedo and surface net radiation that indicates the

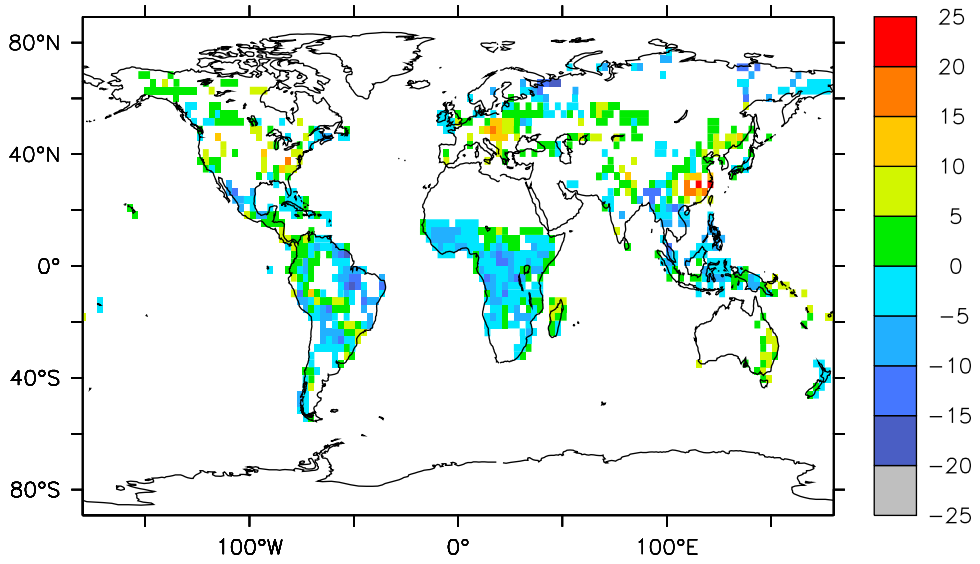

Figure 6. Absolute difference between the future and present-day 4 year mean net surface radiation (W m^{-2}) (calculated as IMG-2050-lucc – IMG-2000) over regions with a change in forest fraction >0.05.

importance of changes in cloud cover caused by changes in momentum, energy and moist exchange, and atmospheric circulation. Similarly, there is no significant correlation between changes in the 4 year mean LE and parameters that one would expect to affect LE, such as changes in surface net radiation and biomass. Figure 7 shows that there are some regions (e.g., in central Africa) where the model simulates a substantial decrease in latent heat flux for 2050 compared to the present. However, over South America, we identify regions with decreases as well as increases in LE. The decrease in evapotranspiration does not always result in an anticipated increase in the sensible heat flux. Over particular regions, such as west and south of the Amazon basin, the decrease in net radiation and turbulence results in a decrease in the sensible heat flux despite the substantial decrease in evapotranspiration. To illustrate the impact of the land cover and land use changes on the energy partitioning, we show in Figure 8a the simulated relative changes in the ratio of sensible to the latent heat flux, the so-called Bowen ratio. Similar to the previously shown changes in surface net radiation and latent heat flux, there is no distinct spatial pattern in the changes in Bowen ratio in relation to land cover and land use changes. Comparison of the spatial distribution of changes in the Bowen ratio with that of the 4 year mean boundary layer depth, shown in Figure 8b, indicates a reasonable correlation between the Bowen ratio and BL depth. Changes in BL depth are relevant to this analysis because they determine the volume in which the

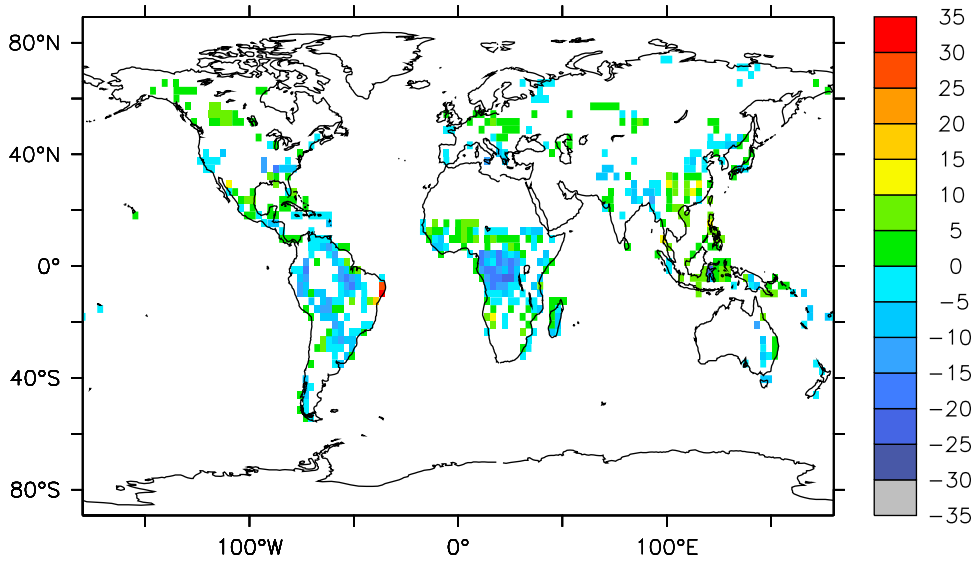

Figure 7. Absolute difference between the future and present-day 4 year mean latent heat flux (W m^{-2}) (calculated as IMG-2050-lucc – IMG-2000) over regions with a change in forest fraction >0.05.

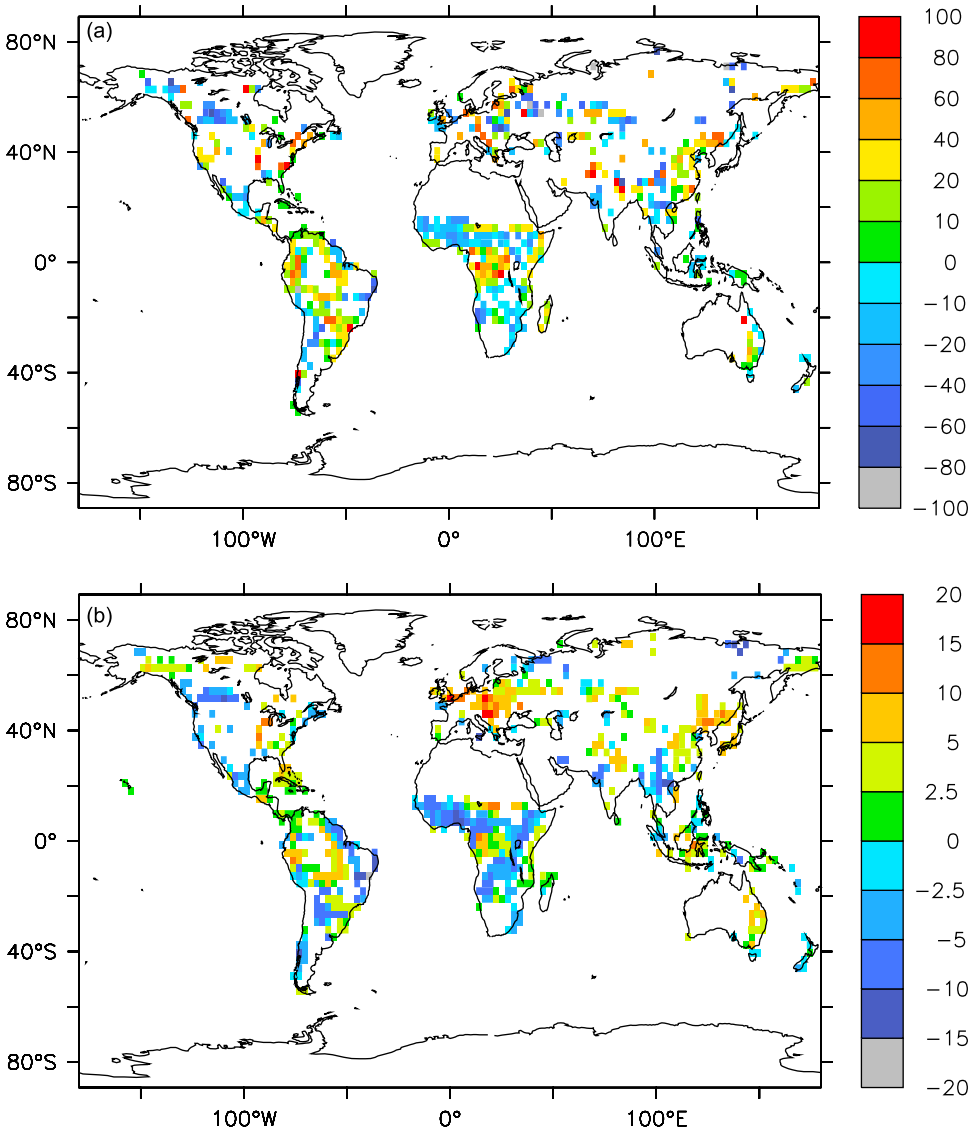

Figure 8. Relative difference (%) between future and present-day 4 year mean (a) Bowen ratio (calculated as 100 × (IMG-2050-lucc – IMG-2000)/IMG-2000) and relative difference between the 4 year mean (b) planetary boundary layer depth, both over regions with a change in forest fraction >0.05.

emitted and deposited chemical compounds interact and the efficiency of exchange between the BL and free troposphere. An increase in the Bowen ratio, and thus an increase in heat relative to moist input to the BL, generally results in an increase in the BL depth (e.g., over the deforested areas in South America and Africa). There are other regions (e.g., northeastern South America and north, east, and south of the African deforested region) where a decrease in the Bowen ratio results in a decrease in BL depth up to about 20% in 2050 compared to the present. However, the correlation coefficient is close to zero, indicating that there is no clear direct relationship between BL depth and LUCC-induced changes in surface energy partitioning. The simulated change in the 4 year mean surface temperature attributed to land cover and land use changes indicates maximum increases as well as decreases up to 2.5 K (Figure 9). However, the global mean surface temperature change caused by land cover and land use change between 2000 and 2050 is negligible in our simulations (~0.03 K). This suggests that these local to regional-scale changes mostly reflect changes in circulation, for example, the locations of low- and high-pressure systems at higher latitudes. Overall, it appears that, in contrast to the clear signal of the changes in land cover and land use in biogenic emissions and dry deposition, that some of main physical drivers of surface and boundary layer exchange of reactive compounds reflect a complex response because of the role of atmospheric circulation and cloud processes.

3.2.4. Atmosphere-Biosphere Exchange

[31] So far, we have discussed the key impacts of land cover and land use changes on biogenic emissions, dry deposition, and micrometeorological and BL meteorological drivers of exchange. Figure 10 shows simulated changes between the present-day and future O_3 atmosphere-biosphere exchange flux. Note that a negative atmosphere-biosphere flux (e.g., for O_3) reflects a dry deposition flux,

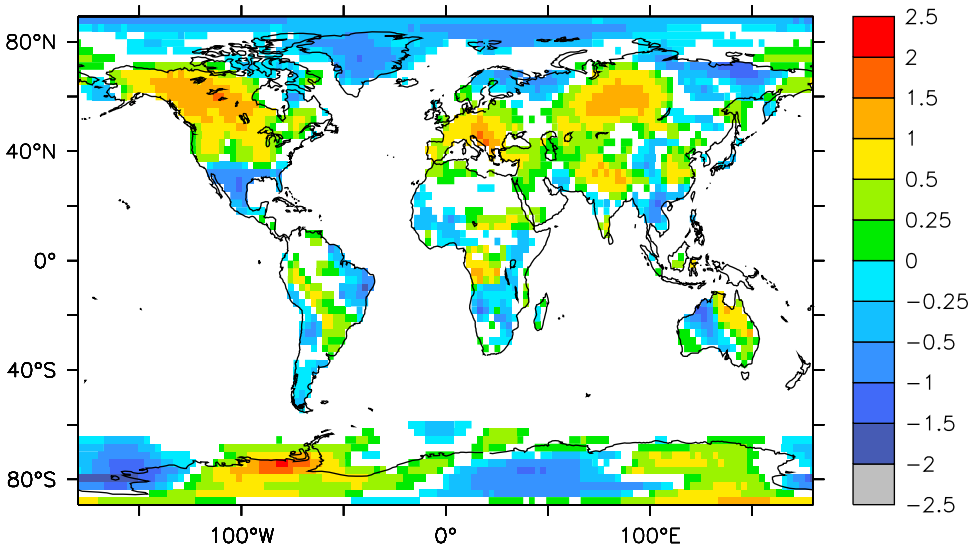

Figure 9. Absolute difference between the future and present-day 4 year mean surface temperature (K) (calculated as IMG-2050-lucc – IMG-2000).

whereas a positive flux reflects emission to the atmosphere. In addition, canopy interactions have only been considered for a canopy height >1 m, whereas the atmosphere-biosphere flux over vegetation <1 m resembles the net flux resulting from dry deposition and biogenic emissions calculated according to the big-leaf approach. Since changes in the O_3 dry deposition flux are calculated as IMG-2050-lucc – IMG-2000, it implies that negative values in Figure 10 reflect an increase in the simulated 2050 O_3 dry deposition flux compared to the present day, and vice versa.

[32] Despite the substantial decreases in V_{dO3} because of tropical deforestation, as shown above, the model only simulates a significant decrease in O_3 deposition in some locations in the periphery of the Amazon forest. Over the vast deforestation regions of central Africa, the model actually simulates an increase in O_3 dry deposition fluxes despite a substantial decrease in V_{dO3}. This indicates a compensating effect through an increase in O_3 surface layer concentrations (see section 3.3). These relatively small changes in O_3 dry deposition fluxes, also caused by these compensating effects, are also reflected by a small decrease in the global integrated atmosphere-biosphere flux of O_3 from approximately −679 Tg O_3 yr^{-1} for the present day to approximately −667 Tg O_3 yr^{-1} for 2050 land cover and land use.

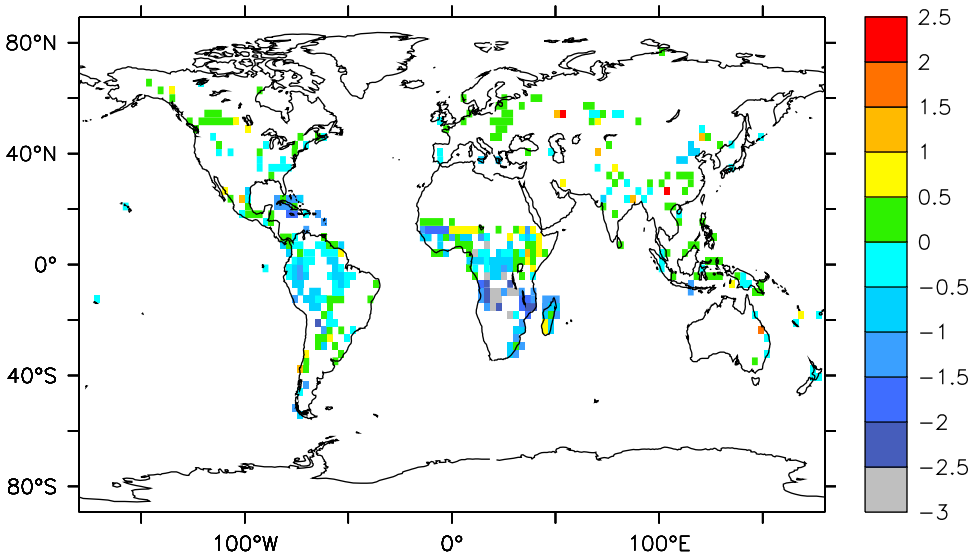

Figure 10. Absolute differences between the future and present-day 4 year mean O_3 atmosphere-biosphere flux (10^{15} molecules m^{-2} s^{-1}) (calculated as IMG-2050-lucc – IMG-2000) over regions with a change in forest fraction >0.05. Note that negative values reflect an increase in the simulated 2050 O_3 dry deposition flux compared to the present, and vice versa (because the downward dry deposition flux is a loss process).

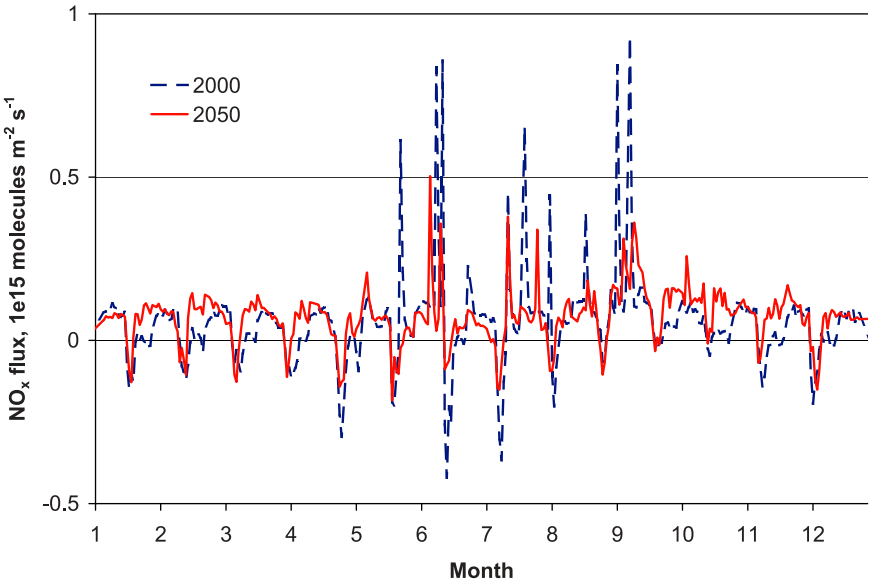

Figure 11. NO_x atmosphere-biosphere exchange flux (10^{15} molecules m^{-2} s^{-1}) for 1 year, representative for present-day conditions (dashed blue line) and future land cover and land use (solid red line) at the location 65°W–15°S at the southern periphery of the Amazon forest. A positive flux reflects an upward (emission) flux, whereas a negative flux reflects a downward (deposition) flux. Note that the temporal variability within 1 month approximately reflects the simulated diurnal cycle in NO_x fluxes because of the use of a 25 h output frequency.

[33] Dry deposition of isoprene, mostly through the uptake by soils [*Cleveland and Yavitt*, 1997], provides only a minor sink of this compound as the emissions are concentrated in the sunlit crown layer. In addition, there will be some within-canopy chemical destruction of isoprene through its reaction with OH (and ozone), but this loss process is relatively slow compared to turbulent transport out of the canopy. This is also reflected by an explicitly simulated ratio of the canopy top to the emission flux (F_{canopy}/F_{emis}), the so-called canopy reduction factor (CRF) [*Yienger and Levy*, 1995], of ~0.95. It indicates that 95% of the leaf-level-emitted isoprene flux of 395 TgC yr^{-1} actually escapes the canopy, with the remaining 5% being removed because of deposition and oxidation inside the canopy. The 2050 long-term mean isoprene CRF is also 0.95, indicating that there is no substantial change in the role of in-canopy chemical destruction and deposition of isoprene associated with land cover and land use changes.

[34] Interpretation of land cover and land-use change impacts on atmosphere-biosphere NO_x exchange is not straightforward. This is related to the bidirectional exchange of NO_x with canopy-top emissions occurring at locations remote from anthropogenic sources and deposition prevailing in regions influenced by anthropogenic sources [*Ganzeveld et al.*, 2002]. The present-day globally integrated NO_x atmosphere-biosphere flux is ~5.2 Tg NO-N yr^{-1}, indicating that the global terrestrial biosphere is a source of NO_x. This source increases by about 30% to ~6.9 Tg NO_x-N yr^{-1} in 2050 because of land cover and land use changes. This increase in the biogenic terrestrial source of about 1.7 Tg NO_x-N yr^{-1} reflects the net effect of a 9% increase in global annual soil NO emission (~1.1 Tg NO-N yr^{-1}) and changes in dry deposition and within-canopy chemical transformations. Apparently, the land cover and land use changes result in an enhanced release of about 0.6 Tg NO_x-N yr^{-1} from the biosphere into the atmosphere. Figure 11 shows the simulated present-day and 2050 canopy-top NO_x fluxes for 1 year for the grid 65°W–15°S in the southern Amazon region to illustrate the simulated impact of deforestation on local-scale atmosphere-biosphere NO_x exchange. Simulated canopy-top NO_x fluxes are generally positive, suggesting that for this site the canopy is a source of NO_x with an annual mean canopy-top NO_x flux of 0.39×10^{14} molecules NO m^{-2} s^{-1}. Only in the early morning does the model simulate small negative fluxes reflecting deposition of NO_x, which has accumulated under the nocturnal inversion and which is removed within the canopy as soon as the inversion breaks down. For this location, the impact of deforestation is reflected by a decrease in the 4 year mean present-day and future LAI from ~4.5 to ~2.3 m^2 m^{-2}, respectively. In addition, the conversion of tropical rain forest to agricultural fields results in a decrease in the simulated 4 year mean soil NO emission flux from 2.3 to 1.5×10^{14} molecules NO m^{-2} s^{-1}. However, this ~30% decrease in the soil NO emission does not result in a substantial decrease in the atmosphere-biosphere NO_x flux. The 4 year mean canopy-top flux for 2050 actually increases to 0.58×10^{14} molecules NO m^{-2} s^{-1}. This increase in the amount of NO_x being released from the canopy reflects a less efficient in-canopy removal of NO_x by chemistry and dry deposition expressed by a present-day local CRF_{NOx} of ~0.2 (0.39/2.3) compared to a 2050 CRF_{NOx} of ~0.4 (0.58/1.5).

3.3. Atmospheric Chemistry and Climate

3.3.1. LUCC Alone

[35] The above discussed changes in atmosphere-biosphere exchanges and the micrometeorology and boundary layer meteorology associated with land cover and

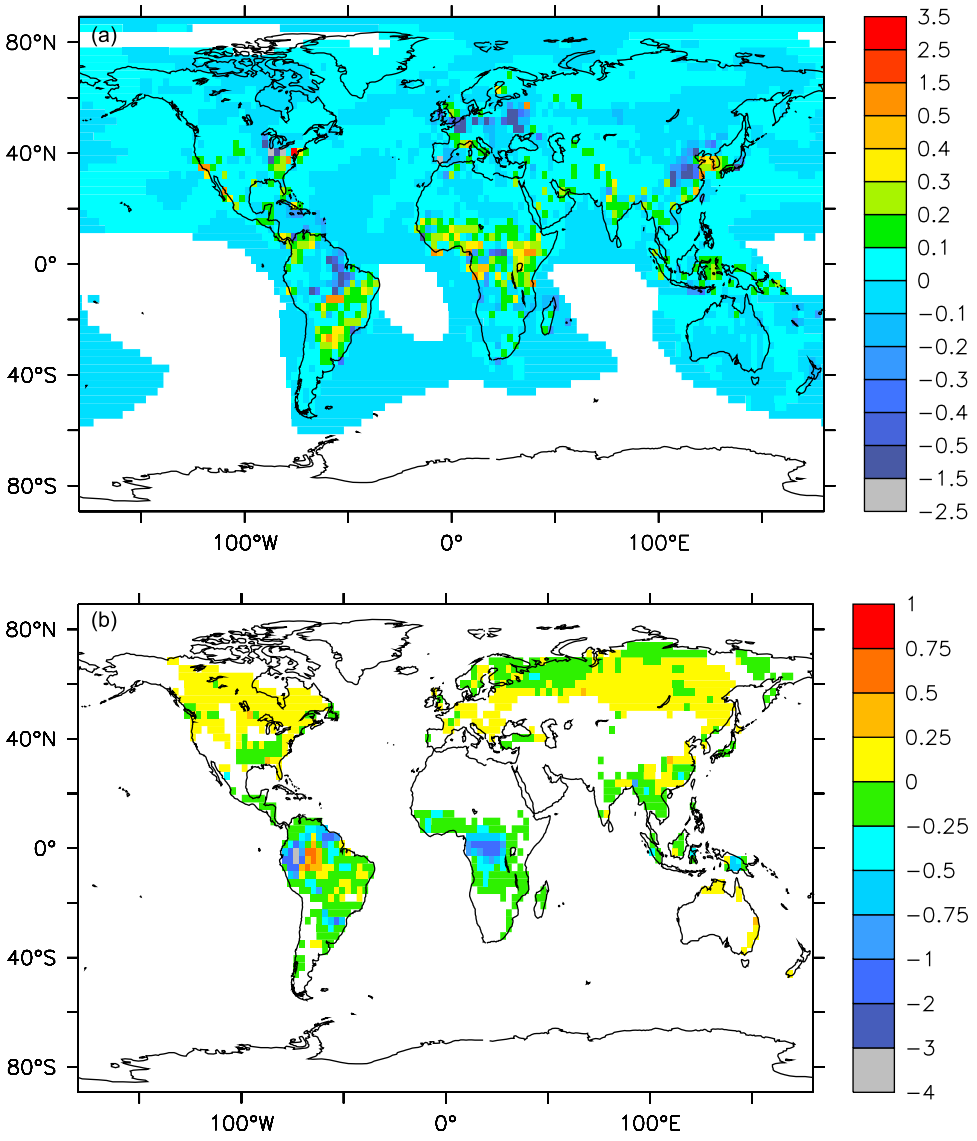

Figure 12. Absolute differences between the future and present-day 4 year mean boundary layer (a) NO_x and (b) isoprene mixing ratios (calculated as IMG-2050-lucc – IMG-2000). Differences are only shown where present-day NO_x mixing ratios are >10 pptv and where isoprene mixing ratios are >50 pptv.

land use changes affect photochemistry and the atmospheric oxidizing capacity through changes in OH and O_3 precursor concentrations and the removal of oxidation products. Figures 12a and 12b show the absolute changes in future mean boundary layer NO_x and isoprene mixing ratios compared to the present. The simulated decreases in soil-biogenic NO and VOC emissions in South America and central Africa result in substantial decreases in the BL NO_x and isoprene mixing ratios. In contrast, simulated increases in NO_x and isoprene mixing ratios over North America and Russia between the future and the present do not correlate with any substantial increases in biogenic emissions. This points to changes in the photochemistry related to simulated changes in the drivers of atmospheric chemistry. The consequences of these changes in the precursor mixing ratios attributed to land cover and land use changes for O_3 and OH are shown in Figures 13a and 13b, respectively. Although there are significant local changes in both O_3 and OH, the main consequences of land cover and land use changes on photochemistry and the atmospheric oxidizing capacity are confined to the tropics where most of the anticipated deforestation will occur. The shown maximum relative changes in O_3 of ~20% resemble absolute changes in the 4 year planetary boundary layer average mixing ratios of ~6 and 9 ppbv for O_3 mixing ratios of ~30 and 45 ppbv over the Amazon forest and central African rain forest, respectively. Simulated changes in O_3 and OH concentrations are also confined to the tropical boundary layer as indicated by relative increases in OH >50% up to an altitude of about 1–1.5 km over South America and central Africa at the equator.

3.3.2. LUCC Versus Anthropogenic Emission Changes

[36] We also conducted a simulation in which we considered changes in land use and land cover as well as changes in anthropogenic emissions (IMG-2050-lucc&emis) to assess the role of land cover and land use changes relative

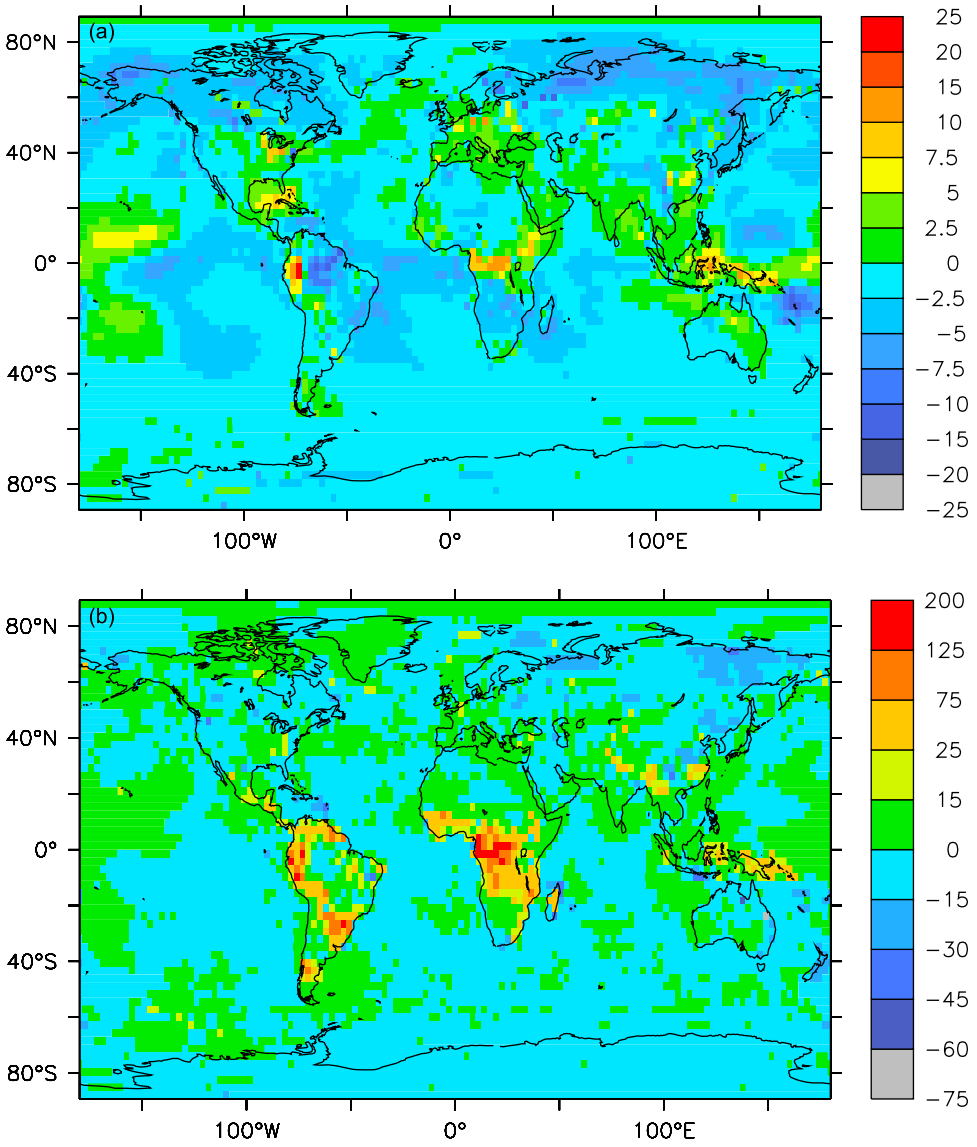

Figure 13. Relative differences between the future and present-day 4 year mean boundary layer (a) O_3 mixing ratios and (b) OH concentrations (calculated as 100 × (IMG-2050-lucc – IMG-2000)/IMG-2000).

to the role of changes in anthropogenic emissions in atmospheric chemistry-climate interactions. Anticipated increases in the 2050 A2 anthropogenic emissions of NO_x, CO, and other O_3 precursors result in large increases in the mean mixing ratios in the boundary layer up to about 30 ppbv of NO_x and more than 200 ppbv of CO over vast regions of eastern and southwestern Asia, India, and the Middle East compared to the present day. More localized increases in anthropogenic emissions are found along the north African Mediterranean coast (e.g., the Nile delta) and around the large urban areas in developing countries (e.g., Nigeria, southeastern South Africa, Santiago, Buenos Aires, and Mexico City). In contrast, the anthropogenic emissions of NO_x and CO are expected to substantially decrease for Europe, Japan, and North America in the future.

[37] The simulated increases in the O_3 precursor emissions between 2000 and 2050 results in a substantial increase of the simulated 4 year mean O_3 mixing ratio in the boundary layer over northwest and northeast Africa, Nigeria, the Middle East, India, and southwestern Asian countries. The maximum increase reaches up to ~30 ppbv. Simulated O_3 mixing ratios also increase over northwest South America and along the west coast of Central America. The 2050 anthropogenic emission scenario results in a maximum simulated decrease in surface layer O_3 of about 10 ppbv over eastern China, despite a substantial increase in NO_x and CO BL mixing ratios. This counterintuitive outcome reflects, in particular, chemical processing for nighttime and wintertime stable BL mixing conditions. Relatively low O_3 mixing ratios prevailing for those conditions are caused by efficient titration of O_3 because of the assumption that all NO_x emissions take place in the form of NO. We note that, to some degree, this might be an artifact of this assumption and the artificial instantaneous mixing over the 2.8° grid cell that requires further studies with more detailed models.

[38] To compare the land cover and land use change-induced influences on atmospheric chemistry with those associated with anthropogenic emissions, we show in

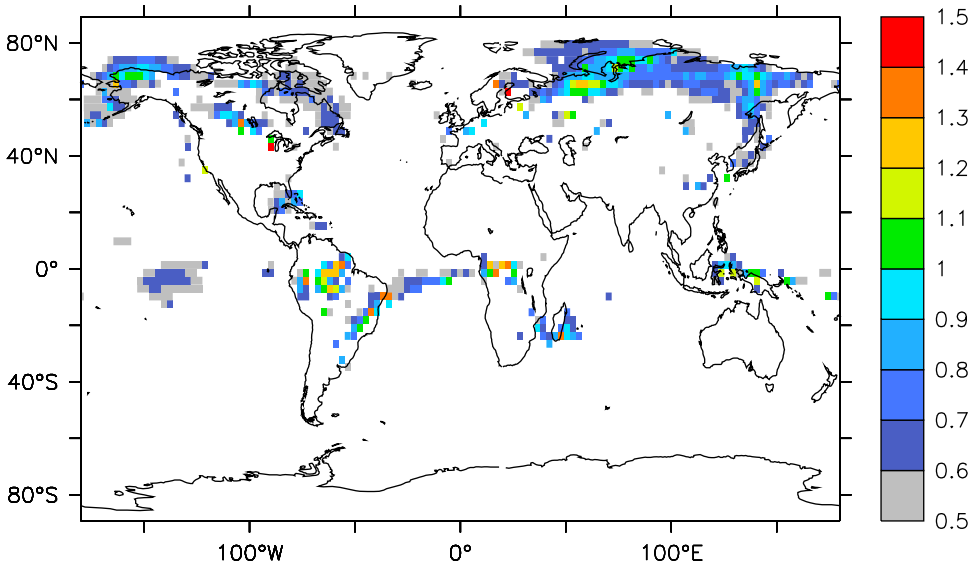

Figure 14. Significance of land cover and land use changes between the present and 2050 for the 4 year BL mean O_3 mixing ratios relative to the overall change in O_3 mixing ratios associated with land cover, land use, and anthropogenic emission changes all together. The relative contribution is only shown for O_3 mixing ratio changes larger than 5% of the absolute O_3 mixing ratio. Values around 1 indicate that land use and land cover changes are the main cause of the changes in O_3, whereas values very different from 1 indicate that anthropogenic emission changes mainly explain the change in O_3.

Figure 14 the relative contribution of LUCC-related changes in O_3 mixing ratios compared to those by the sum of LUCC and anthropogenic emission changes. A ratio of 1 indicates that the changes in BL O_3 are completely controlled by land cover and land use changes, whereas values substantially different from 1 indicate that changes in O_3 are attributed to changes in anthropogenic emissions. For example, a value of 0.5 suggests that the land-cover- and land-use-induced changes in O_3 are reduced by about 50% because of the changes in anthropogenic emissions. Interestingly, this indicates that the regions where the largest consequences of land-use and land cover changes on atmospheric chemistry (and climate interactions) occur are not confined to the tropical forests of South America, Africa, and Asia but that land use and land cover changes are actually also predicted to play an important role in controlling high-latitude atmospheric chemistry. However, the absolute changes in high-latitude mixing ratios of O_3 and its precursors are much smaller compared to the simulated changes in the tropics.

[39] Finally, to indicate how land use, land cover, and anthropogenic emission changes affect atmospheric chemistry-climate interactions, we show in Figure 15 the simulated changes in the 4 year mean seasonal cycle in the methane lifetime, which reflects changes in the atmospheric oxidation capacity. The small differences between the IMG-2000 and IMG-2050-lucc CH_4 lifetime indicate that future land use and land cover changes are not expected to significantly affect the global atmospheric oxidation capacity. Anticipated future increases in anthropogenic emissions result in an increase of the oxidation capacity

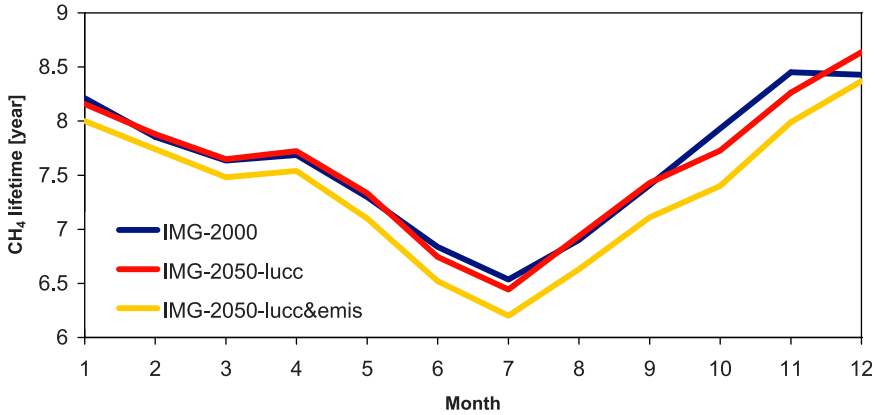

Figure 15. Simulated changes in seasonal cycle in CH_4 lifetime (years) as a function of land use and land cover and anthropogenic emission changes between the present and 2050.

and, consequently, a decrease of the annual mean CH_4 lifetime from about 7.6–7.3 years, a decrease of about 4%.

4. Conclusions

[40] Our analysis of the impact of anticipated future land cover and land use changes on the exchange of reactive compounds, atmospheric chemistry, and meteorology shows that many processes and parameters are significantly affected. For example, large-scale tropical deforestation results in a substantial decrease in foliage VOC emissions and removal of O_3 by deposition because of a decrease in turbulent exchange and foliage uptake. However, also through consistent consideration of process interactions such as the explicit simulation of canopy interactions as a function of key drivers, it appears that the overall impact of land cover and land use changes on reactive trace gas exchanges and atmospheric chemistry is not very large because of compensating effects. A decrease in soil NO emissions for cleared tropical forest land is locally compensated by a decrease in NO_2 foliage uptake. The large-scale decrease in soil-biogenic NO_x from tropical deforested regions is compensated by an increase in emissions associated with fertilizer and animal manure application for managed ecosystems. Deforestation results in a reduced oxidation of isoprene by O_3 and, consequently, in an increase in O_3 concentrations. This also explains a simulated increase of the O_3 deposition flux despite a decrease in the efficiency of O_3 surface removal following forest clearing. Recognizing the potential importance of O_3 dry deposition for climate through its impact on the global carbon sink [*Sitch et al.*, 2007], it stresses the importance of considering these generally ignored features of chemistry-climate interactions in response to land cover and land use changes.

[41] To properly account for these compensating effects, it is required to consistently include the role of the key physical, chemical, biological, and human drivers of reactive compound exchanges. The simulations of biogenic emissions, dry deposition, and canopy interactions in our analysis consider many of these drivers. However, our analysis still relies, to a large extent, on the application of parameterizations and semiempirical models (e.g., the model for soil NO emissions). It is open to discussion whether such approaches are valid for future conditions. The present study also does not include the role of CO_2 in the regulation of isoprene emissions [e.g., *Arneth et al.*, 2007; *Wilkinson et al.*, 2009] nor a differentiation in VOC emissions dependent on land use. This is caused by the limited knowledge of VOC emissions from managed ecosystems in view of the small number of observations. In our study, tropical deforestation results in a substantial decrease in isoprene emissions from managed land because of a substantially smaller average emission factor for all managed ecosystems, according to *Guenther et al.* [1995], compared to that of tropical forest. *Hewitt et al.* [2009] actually demonstrated that palm oil plantations are a large source of isoprene, which, dependent on management practices with respect to N application, has potentially important consequences for air quality and vegetation feedback through ozone production and deposition. Finally, recognizing that land cover and land use change (e.g., tropical deforestation) occurs, to a large extent, on an EMAC subgrid scale implies that our analysis does not include potentially relevant local-scale interactions between surface and boundary layer exchange processes.

[42] Apart from the compensating effects, our approach based on state-of-the-art knowledge about surface exchange processes shows that land cover and land use change are expected to be most important for atmospheric chemistry-climate interactions in background tropical and high-latitude regions. Consequently, our analysis should be extended by downscaling studies based on the application of regional climate or large eddy simulation models that interactively simulate atmospheric chemistry processes similar to the presented approach. These models should further incorporate mechanistic representations of surface exchange processes, including in-canopy interactions, being constrained by high-resolution land management data, to study the impact of land cover and land use changes on chemistry-climate interactions in greater detail.

[43] **Acknowledgments.** We kindly acknowledge the contributions by the colleagues at the Max-Planck Institute for Chemistry (Mainz, Germany) to the development and application of the EMAC model system. L.G. particularly acknowledges the Integrated Land Ecosystem-Atmosphere Processes Study, core project of the International Geosphere-Biosphere Programme, and the scientific steering committee discussions. We also thank three reviewers for their constructive comments.

References

Alcamo, J., E. Kreileman, M. Krol, R. Leemans, J. Bollen, J. V. Minnen, M. Schaeffer, S. Toet, and B. de Vries (1998), Global modelling of environmental change: An overview of IMAGE 2.1, in *Global Change Scenarios of the 21st Century, Results from the IMAGE 2.1 Model*, edited by J. Alcamo, R. Leemans, and E. Kreileman, pp. 3–94, Elsevier Sci., Oxford, U. K.

Arneth, A., et al. (2007), Process-based estimates of terrestrial ecosystem isoprene emissions: Incorporating the effects of a direct CO_2-isoprene interaction, *Atmos. Chem. Phys.*, *7*, 31–53, http://www.atmos-chem-phys.net/7/31/2007/, doi:10.5194/acp-7-31-2007.

Bouwman, A. F., L. J. M. Boumans, and N. H. Batjes (2002), Modeling global annual N_2O and NO emissions from fertilized fields, *Global Biogeochem. Cycles*, *16*(4), 1080, doi:10.1029/2001GB001812.

Bouwman, A. F., K. W. van Der Hoek, B. Eickhout, and I. Soenario (2005), Exploring changes in world ruminant production systems, *Agric. Syst.*, *84*(2), 121–153.

Bouwman, A. F., T. Kram, and K. Klein Goldewijk (2006), *Integrated Modelling of Global Environmental Change, An Overview of IMAGE 2.4, Netherlands Environmental Assessment Agency*, MNP, Bilthoven, The Netherlands.

Chase, T., R. Pielke, T. Kittel, R. Nemani, and S. Running (1996), Sensitivity of a general circulation model to global changes in leaf area index, *J. Geophys. Res.*, *101*(D3), 7393–7408, doi:10.1029/95JD02417.

Cleveland, C. C., and J. B. Yavitt (1997), Consumption of atmospheric isoprene in soil, *Geophys. Res. Lett.*, *24*(19), 2379–2382, doi:10.1029/97GL02451.

Cox, P. M., R. A. Betts, C. D. Jones, S. A. Spall, and I. J. Totterdell (2000), Acceleration of global warming due to carbon-cycle feedbacks in a coupled climate model, *Nature*, *408*, 184–187, doi:10.1038/35041539.

Ganzeveld, L., and J. Lelieveld (2004), Impact of Amazonian deforestation on atmospheric chemistry, *Geophys. Res. Lett.*, *31*, L06105, doi:10.1029/2003GL019205.

Ganzeveld, L., J. Lelieveld, and G.-J. Roelofs (1998), A dry deposition parameterization of sulfur oxides in a chemistry and general circulation model, *J. Geophys. Res.*, *103*(D5), 5679–5694, doi:10.1029/97JD03077.

Ganzeveld, L., J. Lelieveld, F. J. Dentener, M. C. Krol, A. F. Bouwman, and G.-J. Roelofs (2002), Global soil-biogenic NO_x emissions and the role of canopy processes, *J. Geophys. Res.*, *107*(D16), 4298, doi:10.1029/2001JD001289.

Ganzeveld, L., J. Valverde-Canossa, G. Moortgat, and R. Steinbrecher (2006), Evaluation of peroxide exchanges over a coniferous forest in a single-column chemistry-climate model, *Atmos. Environ.*, *40*, 68–80, doi:10.1016/j.atmosenv.2006.01.062.

Ganzeveld, L., et al. (2008), Surface and boundary layer exchanges of volatile organic compounds, nitrogen oxides and ozone during the GABRIEL Campaign, *Atmos. Chem. Phys.*, *8*, 6223–6243, doi:10.5194/acp-8-6223-2008.

Guenther, A., et al. (1995), A global model of natural volatile organic compound emissions, *J. Geophys. Res.*, *100*(D5), 8873–8892, doi:10.1029/94JD02950.

Guenther, A., T. Karl, P. Harley, C. Wiedinmyer, P. I. Palmer, and C. Geron (2006), Estimates of global terrestrial isoprene emissions using MEGAN (Model of Emissions of Gases and Aerosols from Nature), *Atmos. Chem. Phys.*, *6*, 3181–3210, doi:10.5194/acp-6-3181-2006.

Hewitt, C. N., et al. (2009), Nitrogen management is essential to prevent tropical oil palm plantations from causing ground-level ozone pollution, *Proc. Natl. Acad. Sci. U. S. A.*, *106*, 18,447–18,451, doi:10.1073/pnas.0907541106.

IMAGE team (2001), *The IMAGE 2.2 Implementation of the IPCC SRES Scenarios, A Comprehensive Analysis of Emissions, Climate Change and Impacts in the 21st Century*, National Institute for Public Health and the Environment, Bilthoven, The Netherlands.

Jöckel, P., R. Sander, A. Kerkweg, H. Tost, and J. Lelieveld (2005), Technical Note: The Modular Earth Submodel System (MESSy) - a new approach towards Earth System Modeling, *Atmos. Chem. Phys.*, *5*, 433–444, doi:10.5194/acp-5-433-2005.

Jöckel, P., et al. (2006), The atmospheric chemistry general circulation model ECHAM5/MESSy1: Consistent simulation of ozone from the surface to the mesosphere, *Atmos. Chem. Phys.*, *6*, 5067–5104, doi:10.5194/acp-6-5067-2006.

Lathière, J., D. A. Hauglustaine, A. Friend, N. De Noblet-Ducoudr'e, N. Viovy, and G. Folberth (2006), Impact of climate variability and land use changes on global biogenic volatile organic compound emissions, *Atmos. Chem. Phys.*, *6*, 2129–2146, http://www.atmos-chem-phys.net/6/2199/2005/.

Lelieveld, J., et al. (2008), Atmospheric oxidation capacity sustained by a tropical forest, *Nature*, *452*, 737–740, doi:10.1038/nature06870.

Lieth, H. F. H. (1975), Primary production of the major vegetation units of the world, in *Primary Productivity of the Biosphere, Ecological Studies 14*, edited by H. Lieth and R. H. Whittaker, pp. 203–215, Springer, New York. 1975.

Millennium Ecosystem Assessment (2005), *Current State and Trends: Findings of the Condition and Trends Working Group, Ecosystems and Human Well-being*, vol. 1, Island Press, Washington, D. C.

Moss, R. H., et al. (2010), The next generation of scenarios for climate change research and assessment, *Nature*, *463*, 747–756, doi:10.1038/nature08823.

Nakicenovic, N., et al. (2000), *Special Report on Emissions Scenarios (SRES)*, Cambridge Univ. Press, Cambridge, U. K.

Olivier, J. G. H., J. A. van Aardenne, F. Dentener, L. Ganzeveld, and J. A. H. W. Peters (2005), Recent trends in global greenhouse gas emissions: Regional trends and spatial distribution of sources, *Environ. Sci.*, *2*, 81–99, doi:10.1080/15693430500400345.

Pitman, A. J., et al. (2009), Land use and climate via the LUCID intercomparison study: Implications for experimental design in AR5, *Geophys. Res. Lett.*, *36*, L14814, doi:10.1029/2009GL039076.

Pozzer, A., P. Jöckel, H. Tost, R. Sander, L. Ganzeveld, A. Kerkweg, and J. Lelieveld (2007), Simulating organic species with the global atmospheric chemistry general circulation model ECHAM5/MESSy1: A comparison of model results with observations, *Atmos. Chem. Phys.*, *7*, 2527–2550, doi:10.5194/acp-7-2527-2007.

Roeckner, E., et al. (2003), The atmospheric general circulation model ECHAM5, in *Part I: Model Description*, *Rep. 349*, Max Planck Inst. for Meteorol., Hamburg, Germany, available at http://www.mpimet.mpg.de.

Sander, R., A. Kerkweg, P. Jöckel, and J. Lelieveld (2005), Technical Note: The new comprehensive atmospheric chemistry module MECCA, *Atmos. Chem. Phys.*, *5*, 445–450, sRef-ID: 1680-7324/acp/2005-5-445.

Sanderson, M. G., C. D. Jones, W. J. Collins, C. E. Johnson, and R. G. Derwent (2003), Effect of climate change on isoprene emissions and surface ozone levels, *Geophys. Res. Lett.*, *30*(18), 1936, doi:10.1029/2003GL017642.

Sitch, S., P. M. Cox, W. J. Collins, and C. Huntingford (2007), Indirect radiative forcing of climate change through ozone effects on the land-carbon sink, *Nature*, *448*, 791–794, doi:10.1038/nature06059.

Strengers, B., R. Leemans, B. Eickhout, B. De Vries, and L. Bouwman (2004), The land-use projections and resulting emissions in the IPCC SRES scenarios as simulated by the IMAGE 2.2 model, *GeoJournal*, *61*, 381–393, doi:10.1007/s10708-004-5054-8.

Tost, H., P. Jöckel, A. Kerkweg, R. Sander, and J. Lelieveld (2006), Technical Note: A new comprehensive SCAVenging submodel for global atmospheric chemistry modelling, *Atmos. Chem. Phys.*, *6*, 565–574, doi:10.5194/acp-6-565-2006.

van Aardenne, J. A., F. Dentener, J. G. J. Olivier, J. A. H. W. Peters, and L. N. Ganzeveld (2005), The EDGAR 3.2 Fast Track 2000 dataset (32FT2000), http://www.mnp.nl/edgar/model/v32ft2000edgar/docv32ft2000/, Emiss. Database for Global Atmos. Res., Bilthoven, The Netherlands.

van Vuuren, D. P., and B. C. O'Neill (2006), The consistency of IPCC's SRES scenarios to recent literature and recent projections, *Clim. Change*, *75*, 9–46, doi:10.1007/s10584-005-9031-0.

van Vuuren, D. P., P. L. Lucas, and H. Hilderink (2007), Downscaling drivers of global environmental change: Enabling use of global SRES scenarios at the national and grid levels, *Global Environ. Change*, *17*(1), 114–130, doi:10.1016/j.gloenvcha.2006.04.004.

Werth, D., and R. Avissar (2002), The local and global effects of Amazon deforestation, *J. Geophys. Res.*, *107*(D20), 8087, doi:10.1029/2001JD000717.

Wesely, M. L., and B. B. Hicks (2000), A review of the current status of knowledge on dry deposition, *Atmos. Environ.*, *34*, 2261–2282, doi:10.1016/S1352-2310(99)00467-7.

Wilkinson, M. J., R. K. Monson, N. Trahan, S. Lee, E. Brown, R. B. Jackson, H. W. Polley, P. A. Fay, and R. Fall (2009), Leaf isoprene emission rate as a function of atmospheric CO_2 concentration, *Global Change Biol.*, *15*, 1189–1200, doi:10.1111/j.1365-2486.2008.01803.x.

Yienger, J. J., and H. Levy II (1995), Global inventory of soil-biogenic NO_x emissions, *J. Geophys. Res.*, *100*(D6), 11,447–11,464, doi:10.1029/95JD00370.

L. Bouwman, B. Eickhout, E. Stehfest, and D. P. van Vuuren, National Institute for Public Health and the Environment, Netherlands Environmental Assessment Agency, 3720 AH Bilthoven, Netherlands.

L. Ganzeveld, Department of Environmental Sciences, Wageningen University and Research Centre, Droevendaalsesteeg 4, 6707 PB Wageningen, Netherlands. (laurens.ganzeveld@wur.nl)

J. Lelieveld, Max-Planck Institute for Chemistry, J.-Joachim-Becher-Weg 27, Mainz, D-55128, Germany.